International Journal of Science, Technology and Society
2017; 5(4): 131-140
http://www.sciencepublishinggroup.com/j/ijsts
doi: 10.11648/j.ijsts.20170504.22
ISSN: 2330-7412 (Print); ISSN: 2330-7420 (Online)

A New Procedure for Porous Material Characterization

Chavdar Chilev[1, 2, *], Yana Stoycheva[1, 2], Moussa Dicko[1], Farida Lamari[1], Patrick Langlois[1], Ivan Pentchev[2]

[1]LSPM CNRS, University Paris 13, Villetaneuse, France

[2]Department of Chemical Engineering, University of Chemical Technology and Metallurgy, Sofia, Bulgaria

Email address:

chavdar_chilev@uctm.edu (C. Chilev), stoycheva@yahoo.com (Y. Stoycheva), moussa.dicko@lspm.cnrs.fr (M. Dicko), farida.lamari@lspm.cnrs.fr (F. Lamari), patrick.langlois@lspm.cnrs.fr (P. Langlois), pentchev@uctm.edu (I. Pentchev)

[*]Corresponding author

To cite this article:

Chavdar Chilev, Yana Stoycheva, Moussa Dicko, Farida Lamari1, Patrick Langlois, Ivan Pentchev. A New Procedure for Porous Material Characterization. *International Journal of Science, Technology and Society*. Vol. 5, No. 4, 2017, pp. 131-140.
doi: 10.11648/j.ijsts.20170504.22

Received: May 28, 2017; **Accepted**: June 22, 2017; **Published**: July 24, 2017

Abstract: A new procedure for quantitative characterization of different types of solid materials is proposed. The technique is based on the Scanning Electron Microscopy (SEM) analysis results of porous materials and their processing by the software *ImageJ*. Several types of porous adsorbents AX21, AC35, GAC250, ACENO and IRH3 activated carbons were investigated. Based on SEM analysis, different characteristics of the samples such as porosity, pore size distribution, bed particles porosity can be obtained. In this study, the particle size, the average macropore size and pore size distributions (PSD) of samples were determined with a new procedure for SEM analysis treatment using *ImageJ* software. Three distribution functions (Gamma, Weibull and Lognormal) were selected to describe the experimental results. The Lognormal distribution fitted more accurately the experimental data.

Keywords: Porous Materials, SEM, PSD, *ImageJ*, Activated Carbon

1. Introduction

Many phenomena occurring at phase boundary fluid-solid cause significant scientific interest and are characterized by a number of practical applications, *i.e.* adsorption, extraction, sublimation, crystallization, etc. In the first two processes, which have found wide application in practice, the solid phase is usually porous [1]. The properties of porous solids depend mainly on their structure and in particular the internal surface, because namely the internal surface determines the distribution of the free surface energy and hence the sorption properties. Activation process of porous sorbents aims at increasing the internal surface of the solid samples. Therefore it is necessary to establish the structure of the porous solids that gives information about the quality of the activation process and the sorption properties of the materials. For technical application within sorption processes it is important to know the structure and the physico-chemical properties of the solid samples such as specific surface area, pore volume and PSD. Different methods to study the basic characteristics of porous solids are used; the pore volume is determined by mercury porosimetry [2, 3], helium displacement measurements [4, 5], t-method [6]; the specific surface area - by BET method [7]; the pore size distribution - by Barrett-Joyner-Halenda method [8], Horvath-Kawazoe method [9], and the sample's surface topography and composition by the SEM analysis [10]. A major part of the SEM analysis is the interpretation of the results. In many cases, the results are purely qualitative and based on them only the type of sample's structure is determined. In this paper a new simple procedure, which necessitates SEM analysis results for further quantitative characterization of the investigated samples was proposed. This technique is based on *ImageJ* software for processing the SEM analysis results. Both the particles and the pores into the particles can be counted, outlined and numbered by the *ImageJ* software. Activated carbons AX21, AC35, GAC250, ACENO and IRH3 were investigated. In order to fully describe the used materials, different operating

conditions of the SEM equipment and different software optimizations were carried out. A procedure to process the SEM results by the *ImageJ* software was proposed. A critical discussion due to the advantages and limitations of this technique was given. Thus, the particle size and the PSD of solid samples were obtained.

2. Materials and Methods

2.1. Porous Materials

Activated carbon has become one of the most technically important and most widely used materials because of its high adsorptive capacity and low cost. In this paper the surface physical morphology of activated carbons AX21, AC35, ACENO, IRH3, and GAC250 by a scanning electron microscopy was investigated. Activated carbon IRH3 was produced from coconut coal by the Hydrogen Research Institute (Canada) and exhibits a surface area of 2600 m^2/g. Activated carbon GAC250 produced from CECA Elf ATOCHEM (France) has a specific area about 1030 m^2/g. AX21 is a petroleum pitch-based activated carbon of high adsorption capacity (2500 m^2/g), manufactured by Anderson Development (Adrian, MI, USA). AC35 (CECA, France) has an average surface area of 900 m^2/g.

2.2. SEM Setup Description

The scanning electron microscope uses a focused beam of high-energy electrons to generate a variety of signals at the surface of solid specimens. The signals that derive from electron-sample interactions reveal information about the sample including external morphology (texture), chemical composition, and crystalline structure and orientation of materials making up the sample. Areas ranging from approximately 1 cm to 5 microns in width can be imaged in a scanning mode using conventional SEM techniques (magnification ranging from 20X to approximately 300000X, spatial resolution from 50 to 100 nm) [11, 12]. SEM devices have at least one detector. The specific potentialities of a particular instrument are critically dependent on which detectors it accommodates [12]. In this study the surface physical morphology of activated carbons was observed by a scanning electron microscopy (SEM, LEICA Cambridge S440 located at Paris 13 University) at accelerating voltages of 5-40 keV with magnification between 50X and 300000X and resolution maximal 5 nm.

2.3. Analysis Method

Image processing is important because it can improve the appearance of the image, bring out obscure details in an image and carry out quantitative measurements [13]. *ImageJ* is a public domain Java image processing program inspired by NIH Image for the Macintosh. The author, Wayne Rasband is at the Research Services Branch, National Institute of Mental Health, Bethesda, Maryland, USA [14-16]. *ImageJ* holds a unique position because it is not only in the public domain, but also runs on any operating system. The source code for *ImageJ* is freely available [17]. It is attractive because it is easy to use, can perform a full set of imaging manipulations and has a huge and knowledgeable user community. Because of the easy way in which *ImageJ* can be extended, using macros and plugging, a lot of functionalities are available today, especially in the fields of microscopy and biology. *ImageJ* can be used to acquire images directly from scanners, cameras and other video sources [18, 19]. User written plugging make it possible to solve many image processing and analysis problems, from three dimensional live-cell imaging [20], to radiological image processing [21], multiple imaging system data comparisons [22] to automated hematology systems [23]. It can calculate area and pixel value statistics of user defined selections, measure distances and angles [24], create density histograms and line profile plots. *ImageJ* supports standard image processing functions such as contrast manipulation, sharpening, smoothing, edge detection and median filtering [25]. Unlike most image processing programs, the software does not have a main work area. The main window of *ImageJ* is actually quite parsimonious containing only a *Menu Bar*, *Menu Commands*, a *Tool Bar* and a *Status Bar*. Images, histograms, profiles, widgets, etc. are displayed in additional windows. Measurement results are displayed in the results Table. Most windows can be dragged around the screen and resized [25-27].

2.4. Processing Application

On Figure 1a one can clearly see the grains of the AC35 sample. Therefore this image can be used to determine the adsorbent grain size.

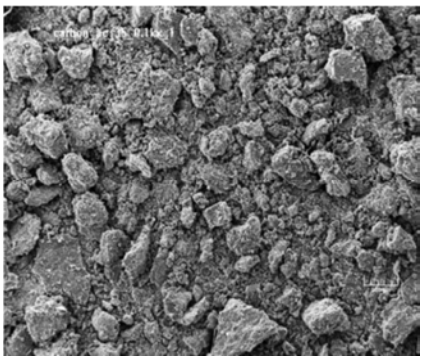

a) 0.1 kX

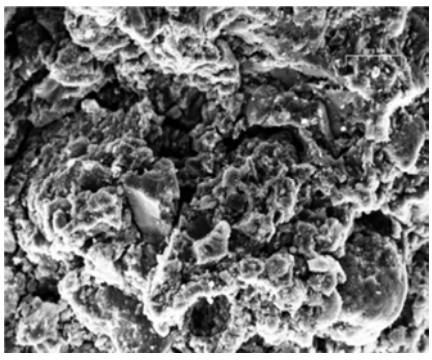

b) 1 kX

Figure 1. *SEM micrographs of the activated carbon AC35 at 0.1 kX (a) and 1 kX (b) magnifications.*

Macropores and cracks on the adsorbent surface can be observed at higher magnification of SEM results corresponding to the same sample (Figure 1b). Thus, Figure1b can be used to determine the macropore size distribution. Using *ImageJ* the received images were processed. The first step is the image calibration required to correlate the image dimensions in pixel to physical dimensions. The image should be converted to 8 bit grayscale (256 gray levels, 0 is pure black, 255 is pure white).

During the SEM analysis, the work sample is illuminated and then an image is taken. In this way part of the objects in the sample includes shadows associated with the illuminated angle. If the contrast of the image is not be changed by *ImageJ*, these shadows will be included in the size of the objects themselves, which then will lead to incorrect results. For example, in Figure1b the purpose is to obtain the macropore sizes that are displayed as absolute black objects. Cracks on the adsorbent surface are also displayed on the Figure1b as absolute black objects. Some macropores are located into the cracks but they are not visible (black objects) and thus they cannot be determined. Therefore the cracks should not be taken into account in the counting of macropores. For this purpose, the contrast of the image (Figure 1b) must be modified.

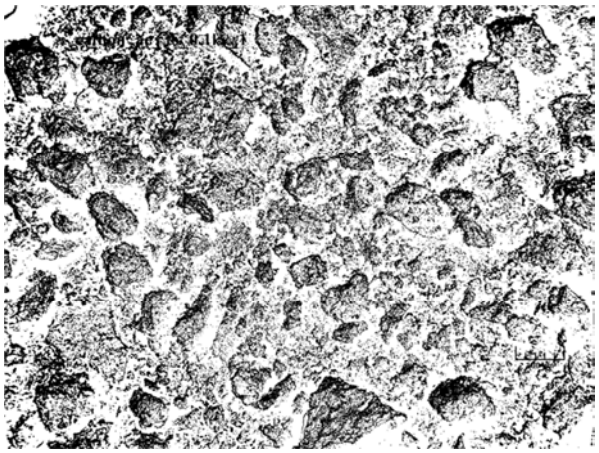

a) from Figure 1a

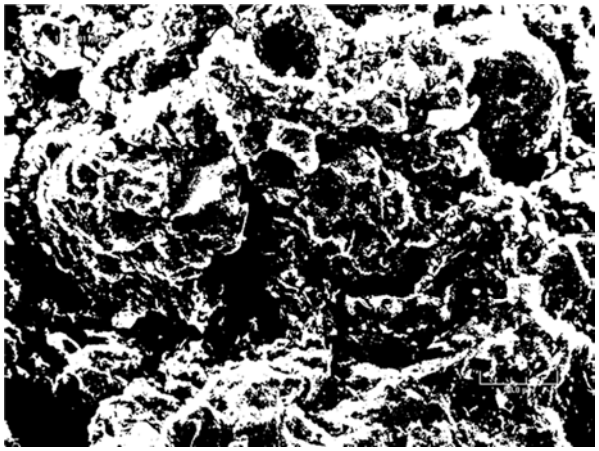

b) from Figure1b

Figure 2. *The thresholded SEM micrographs from Figure 1a and 1b.*

On Figure 2b is displayed the image from Figure 1b with the contrast options applied. In some cases the options for adjustments in contrast are not necessary, only the transformation of the objects in black and white are needed, which is the case of Figure 1a into Figure 2a. On both figures is displayed the emphasis (pure black/pure white - without other gray levels) of the target measurement objects, which is a prerequisite to obtain correct results.

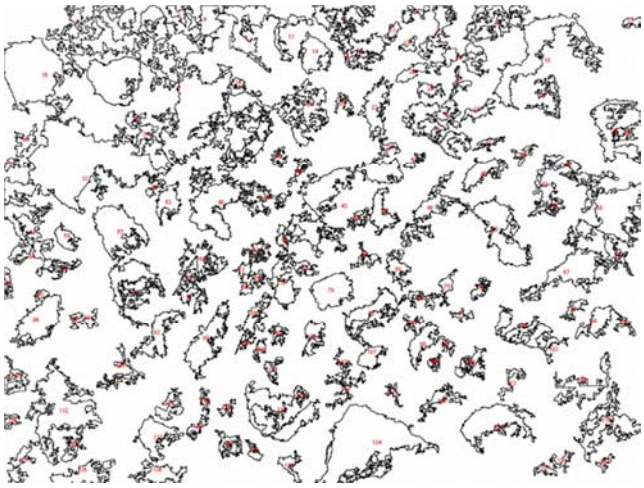

a) Particles

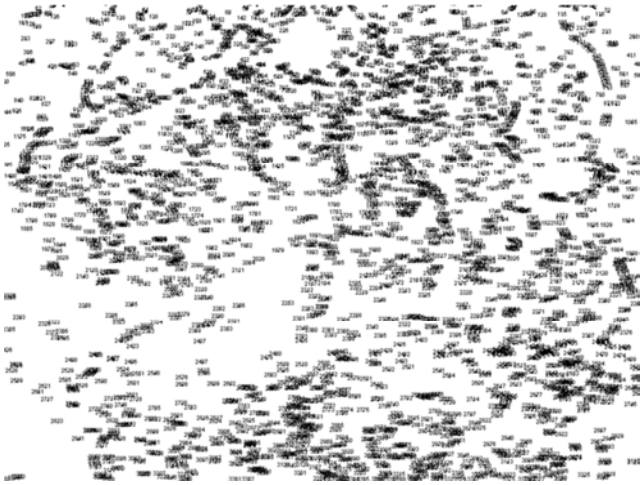

b) Pores

Figure 3. *SEM micrographs with counted, outlined and numbered objects (particles (a) and pores (b)).*

The next step in the analysis is to outline the target objects on the modified image. A very important point in this operation is to specify the size of the target objects. For this purpose upper and lower limits for the objects size must be set. So all chosen objects (particles or pores respectively) will be counted, outlined and numbered.

Figure 3a and Figure 3b show the results of the target objects outlining. Thus, only chosen objects (in this case, the grains size (a) and the macropores size (b)), excluding those with unsuitable size, using the lower (0.5 μm) and upper (300 μm) limits for the object size can be determined.

a) Thresholded image from Figure 1b

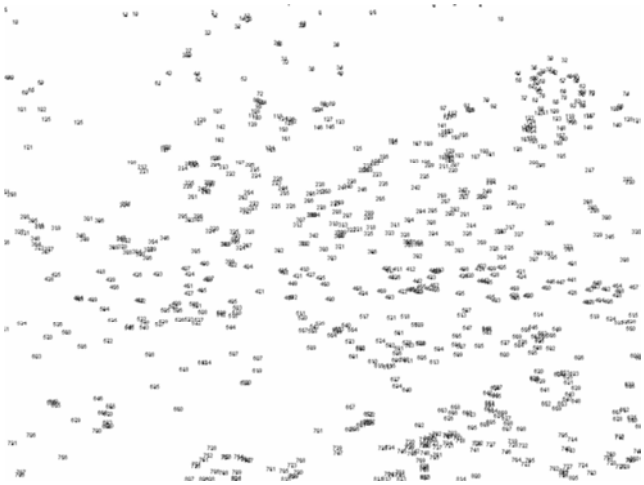

b) Counted objects from Figure 1b

Figure 4. *The thresholded image (a) and the counted objects (b) from Figure 1b which are obtained without adjustment of the image contrast.*

Figure 4a and Figure 4b show the thresholded image and the counted objects from Figure 1b, which are obtained without adjustment of the image contrast, only by transformation of the objects in black and white.

The comparison between Figure 2b and Figure 4a gives the difference in size of the black and white objects. Very large differences in the counted objects numbers and sizes are observed between Figure 3b and Figure 4b. Therefore, preliminary analysis is necessary to determine the appropriate contrast adjustment that is required in the processing of the work sample.

The considered experiment consists in the measurement of object (particle/pore) size and the number of objects with appropriate size. For example, the results from the SEM micrograph of the activated carbon AC35 at 0.1 kX magnification are given. One possibility to visualize these data is to make a histogram.

The Feret's diameter also known as "caliper length" represents the diameter of the circumscribed circle or the longest distance between any two points along the object boundary was obtained. In this work, the "*hist"* function in *MatLab* program environment is used to build the histograms based on the counted objects, sorted by size into groups. Figure 5 shows a histogram, received from the counted objects on Figure 3a. The histogram is presented as a set of (x, y) values, where each x is a bin center and y is a bin height. Thus, it would fit a distribution curve through those points with x object size and y counted objects.

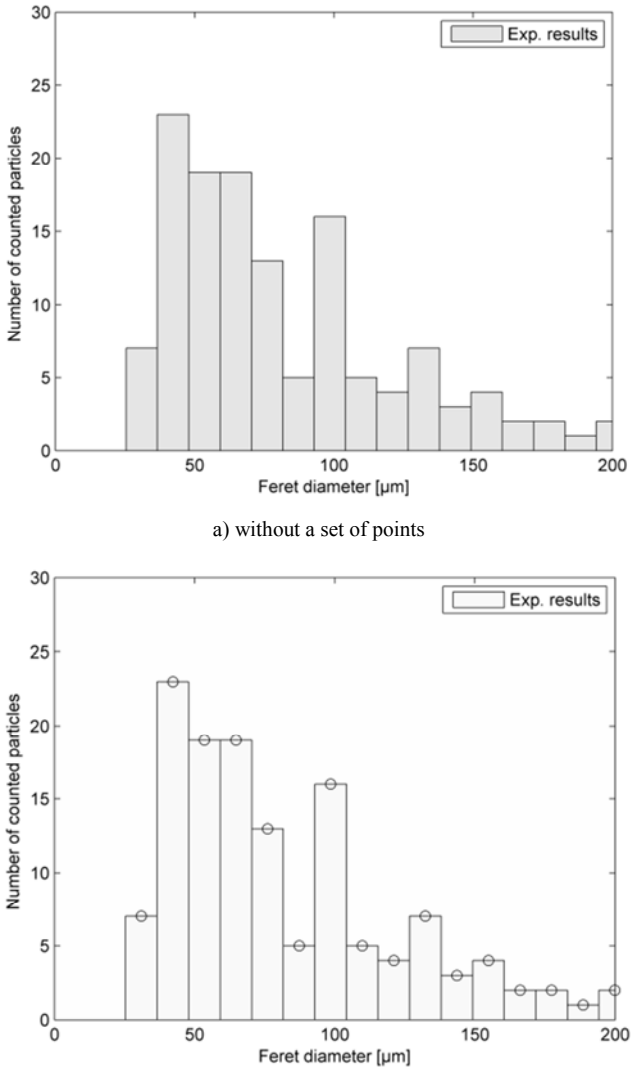

a) without a set of points

b) with a set of points

Figure 5. *Particle size distribution histogram of activated carbon AC35 without a set of points (a) and with a set of points (b).*

It is necessary to notice that the histogram represents a scaled version of an empirical *probability density function* (PDF). Thus, different distribution functions can be used to describe the experimental results. In this work, three distribution functions were selected:

Weibull distribution

$$y = f\left(x \mid a,b\right) = ba^{-b}x^{-b}e^{-\left(\frac{x}{a}\right)^{b}} I_{(0,\infty)}\left(x\right)$$

Gamma distribution

$$y = f\left(x \mid a,b\right) = \frac{1}{b^a \Gamma\left(a\right)} x^{a-1} e^{-\frac{x}{b}}$$

Lognormal distribution

$$y = f\left(x \mid \mu,\sigma\right) = \frac{1}{x\sigma\sqrt{2\pi}} e^{\frac{-\left(\ln(x)-\mu\right)^2}{2\sigma^2}}$$

Figure 6 shows the fits, obtained with the selected distribution functions, and the experimental histograms. The data for the fit coefficients and standard deviations are shown in Table 1.

In Figure 6, the Lognormal distribution gives the best fit to the experimental data, followed by the Gamma distribution. Using the Weibull distribution the results with unsatisfactory accuracy were obtained. The size of linear dimension of the statistical intervals might affect the fit of distribution. Therefore, one can change the size of linear dimension of the statistical intervals. The height of some bins on the figure is bigger than the limits of the diagram, but does not affect the model distributions. The actual bin height values are not shown in the figure for perspicuity reasons and for clearer presentation of the received model distributions. The same procedure was applied to the Figures 10, 12, 15 and 17.

Table 1. *Fit coefficients and standard deviations for the used distributions and porous materials.*

AC35, 0.1kX		
	a	b
Weibull	101,549	1,613
Gamma	3,229	27,893
Lognormal	4,338	0,539
AC35, 1kX		
	a	b
Weibull	0,809	3,244
Gamma	10,176	0,071
Lognormal	-0,374	0,310
ACENO, 1kX		
	a	b
Weibull	42,117	1,152
Gamma	1,659	23,863
Lognormal	3,348	0,725
ACENO, 5kX		
	a	b
Weibull	0,254	1,273
Gamma	2,005	0,116
Lognormal	-1,729	0,656
AX21, 0.5kX		
	a	b
Weibull	50,726	1,563
Gamma	3,044	14,787
Lognormal	3,634	0,542
AX21, 5kX		
	a	b
Weibull	0,260	1,186
Gamma	1,763	0,137
Lognormal	-1,728	0,689
AC35, 0.1kX		
IRH3, 5kX		
	a	b
Weibull	0,229	1,351
Gamma	2,362	0,088
Lognormal	-1,803	0,594
GAC250, 30kX		
	a	b
Weibull	0,064	0,907
Gamma	1,048	0,065
Lognorma	-3,233	0,887

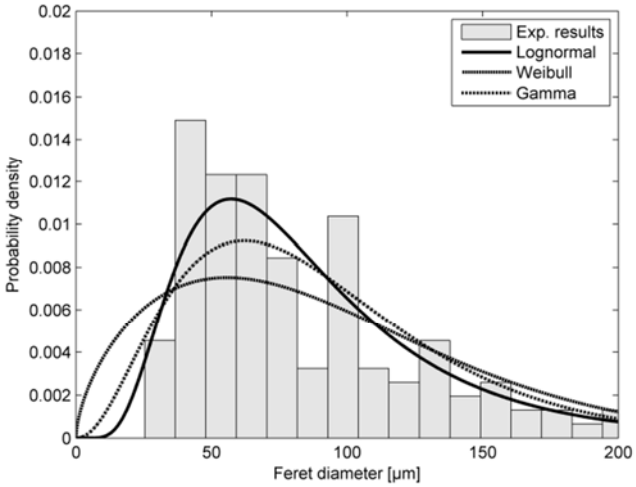

Figure 6. *Particle size distribution of activated carbon AC35.*

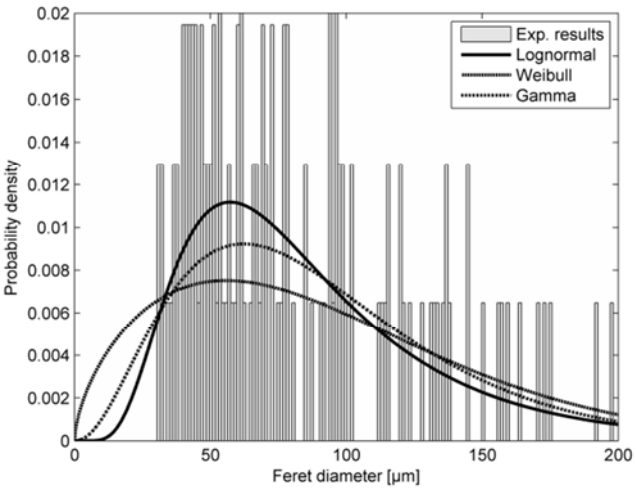

Figure 7. *Particle size distribution of activated carbon AC35 fitted with thirteen time smaller interval size than on the Figure 6.*

Figure 7 displays the same experimental results as on Figure 6, but with thirteen times smaller interval size. The received histogram is fitted with the used distribution functions. In both cases (Figure 6 and Figure 7) the same values for the fit coefficients are obtained. The comparison between the two figures and the values of fitting processes (see Table 1), proves that the size of linear dimension of the statistical intervals does not affect the type of received model distributions. Thus, regardless of how the counted objects are sorted, their size distribution functions remain the same. This

is an indication that the resulting histograms correctly represent the experimental results (SEM).

Thus, we propose the following procedure to obtain a correct result.

(1) Availability of the SEM results with good quality and clear visibility.

(2) Preliminary analysis of the SEM micrographs to determine the desired measurement objects in terms of their contrast and approximate dimensions.

(3) Contrast correction of the image depending on the analysis made in section 2.

(4) Outlining of the chosen measurement objects on the basis of the received contrast image in point 3.

(5) If there is a discrepancy between the result, obtained in section 4 and the analysis made in section 2, it can be proceeded to another change of the image contrast and re-count the objects (repeat steps 3 and 4).

(6) Fitting of the resulting histograms by the selected distribution functions. If there is accordance with the results obtained in section 4 and in section 2, several histograms with different bin sizes may be built.

(7) The fitting results are correct, when the same results by fitting with different bin size are obtained.

Using the above mentioned procedure, size distributions of the targeted measurement objects can be correctly obtained from SEM analyses. The same procedure is applied to the SEM analysis results for all samples.

3. Results and Discussion

3.1. Activated Carbon - AC35

For AC35 the result of the SEM analysis is given in Figure 1a and Figure 1b. Applying the above procedure Weibull, Gamma and Lognormal distributions are obtained (Figure 6 and Figure 7). The data of fit coefficients and standard deviations are shown in Table 1. On the basis of the received distributions an average grain size of 60 µm is determined for AC35.

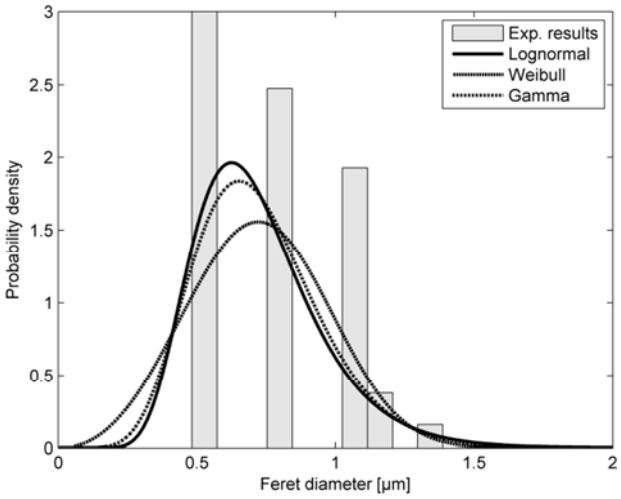

Figure 8. *PSD of activated carbon AC35.*

Figure 8 shows the received PSD distribution functions obtained from Figure 1b. On the basis of these distributions an average macropore size of 0.6 µm for AC35 is obtained.

3.2. Activated Carbon - ACENO

The surface physical morphology of activated carbon ACENO was observed by a scanning electron microscopy with magnification 1 kX and 5 kX

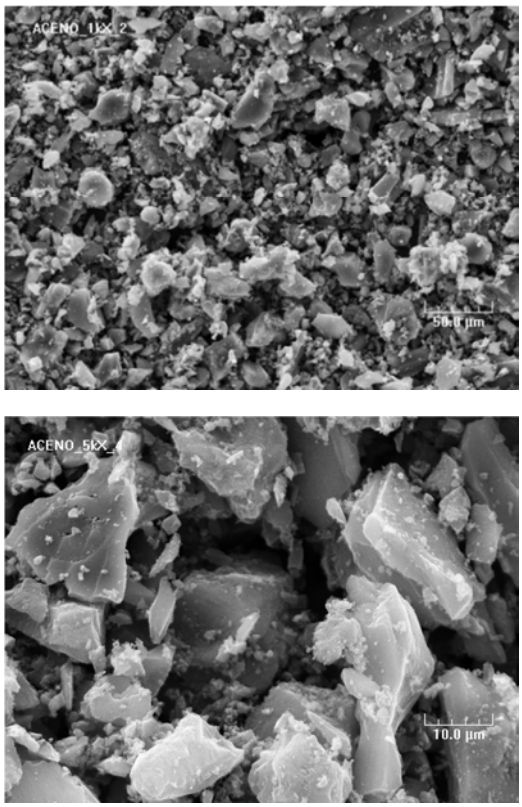

Figure 9. *SEM micrographs of the activated carbon ACENO at 1 kX (a) and 5 kX (b) magnification.*

The Figure 9a is chosen, because one can clearly see the grains of the adsorbent. On Figure 9b the macropores and cracks on the adsorbent surface are visible.

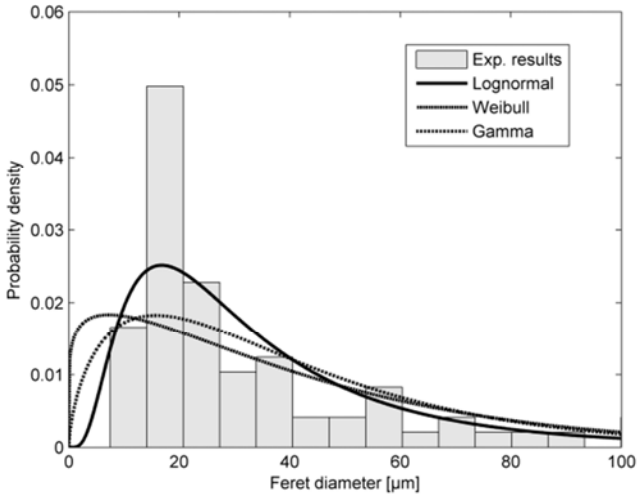

a) Particle size distribution

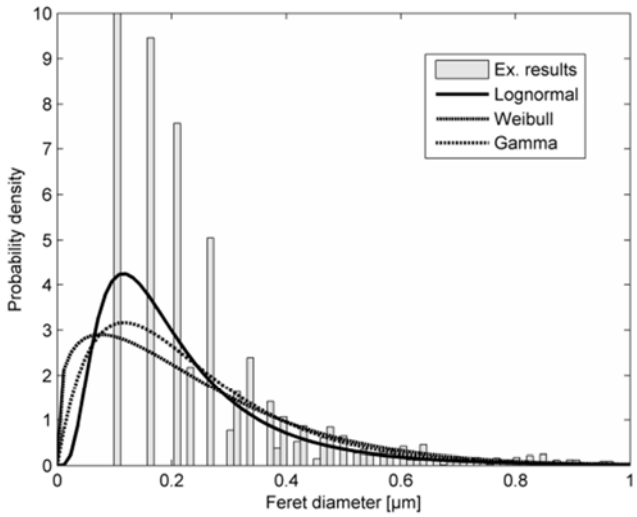

b) PSD

Figure 10. *The obtained distribution of activated carbon ACENO - the particle size distribution (a) and the PSD (b).*

After applying the above algorithm proposed on the images (Figure 9a and Figure 9b) Weibull, Gamma and Lognormal distributions are obtained. For ACENO an average grain size of 20 µm and an average macropore size of 0.1 µm were obtained.

3.3. Activated Carbon – AX21

The surface physical morphology of activated carbon AX21 was observed by a scanning electron microscopy with magnification 0.5 kX and 5 kX (Figure 11a and Figure 11b). The received SEM micrographs can be used to determine the grain and macropore size. On the basis of the received distributions (Figure 12a and Figure 12b) an average grain size of 30 µm and an average macropore size of 0.1 µm for AX21was determined.

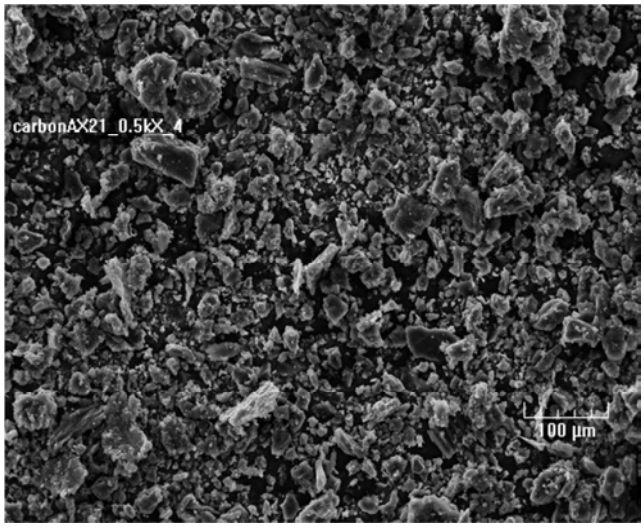

a) 0.5 kX

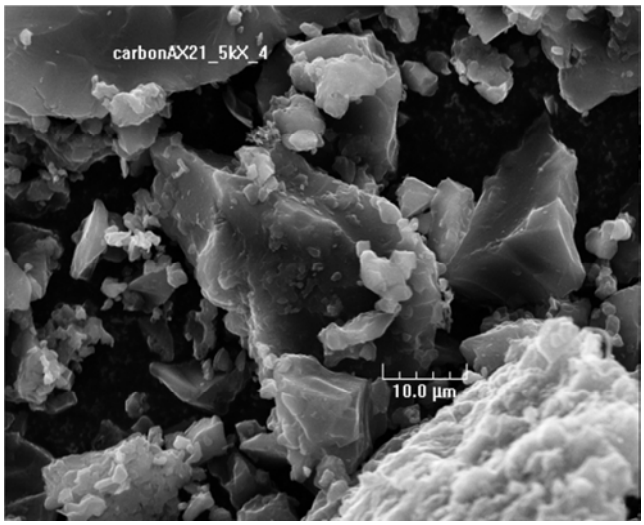

b) 5 kX

Figure 11. *SEM micrographs of the activated carbon AX21 at 0.5 kX (a) and 5 kX (b) magnification.*

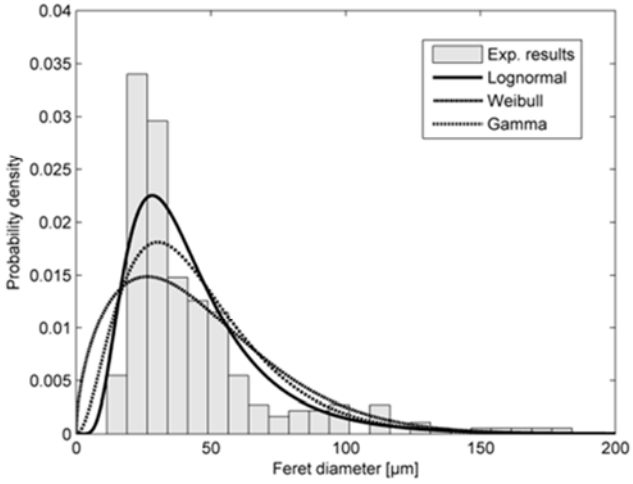

a) Particle size distribution

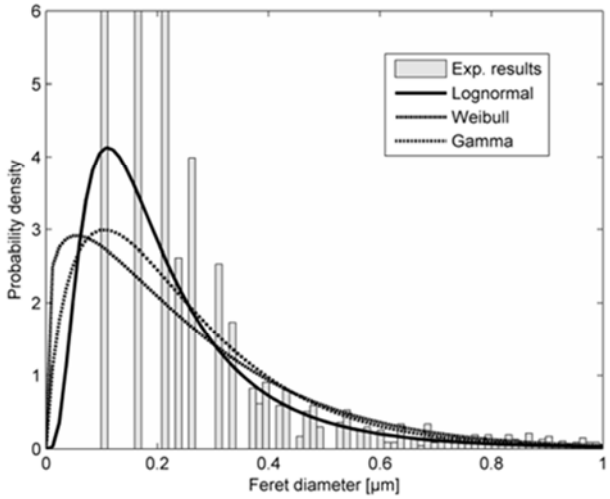

b) PSD

Figure 12. *The obtained distribution of AX21 - the particle size distribution (a) and the PSD (b).*

3.4. Activated Carbon – IRH3

For IRH3 the results of the SEM analysis are given in Figure 13a and Figure 13b.

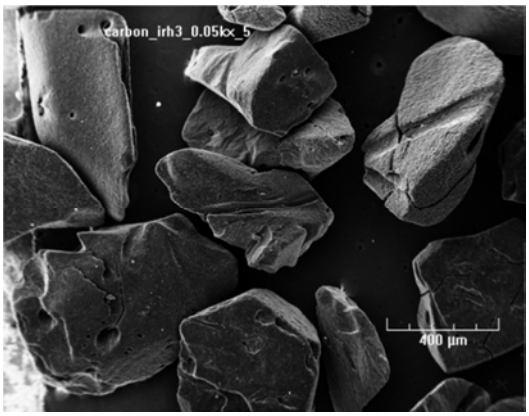

a) 0.05 kX

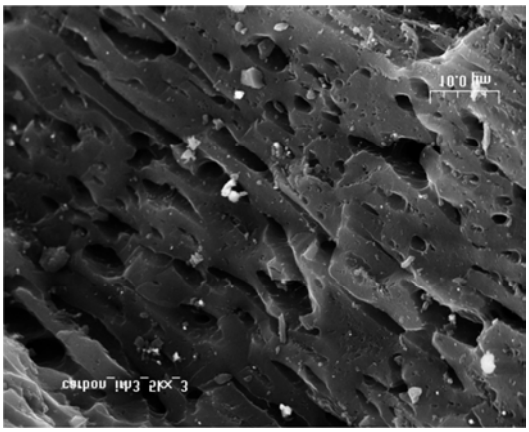

b) 5 kX

Figure 13. *SEM micrographs of the activated carbon IRH3 at 0.05 kX (a) and 5 kX (b) magnification.*

The sample on Figure 13a was so illuminated that part of the objects in the sample incorporates shadows, associated with the angle, at which they are illuminated. To consider this phenomenon, the contrast of the photo was modified (Figure 14a) and the grains in the sample were outlined and counted (Figure 14b).

a) Threshold image

b) Counted objects

Figure 14. *The threshold image (a) and the counted objects (b) from Figure 13a.*

Although the contrast of the image was adjusted, the shadows were included in the size of the objects, this led to incorrect results in the outlined and counted grains. Therefore, although the adjustments made the image from Figure 13a cannot be used for determining of the grain size distribution. The macropore size distribution from Figure 13b was obtained applying the above proposed procedure (Figure 15). On the basis of the received distributions (Figure 15) an average macropore size of 0.1 µm was obtained for IRH3.

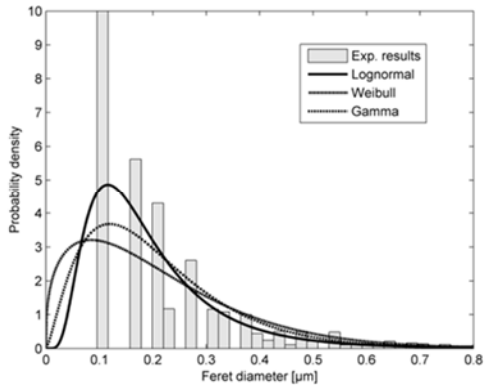

Figure 15. *The particle size distribution of IRH3.*

3.5. Activated Carbon – GAC250

The surface physical morphology of activated carbon GAC250 was observed by a scanning electron microscopy with magnification 0.05 kX and 30 kX.

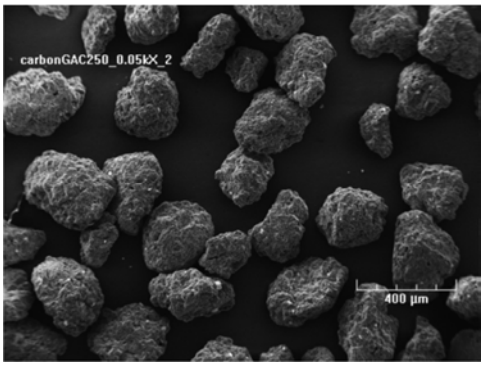

a) 0.05 kX

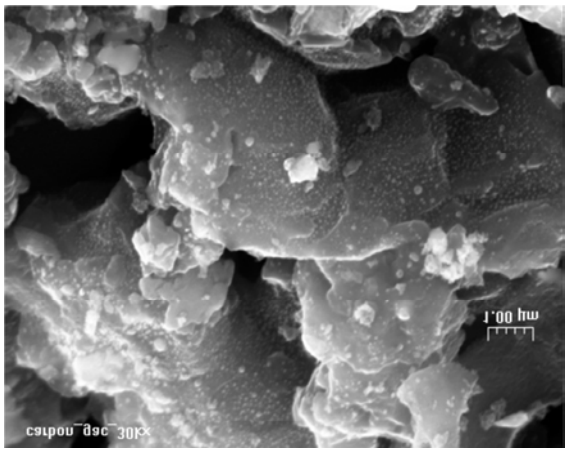

b) 30 kX

Figure 16. *SEM micrographs of the activated carbon GAC250 at 0.05 kX (a) and 30 kX (b) magnification.*

As in the previous case with the activated carbon IRH3, here shadows are included in the size of the objects in the sample (Figure 16a). It led to incorrect results in the outlined and counted grains and thus the particle size could not be determined. The SEM image on Figure 16b can be used to determine the macropore size. Thus, for GAC250 base on the received distributions (Figure 17) an average macropore size of 0.05 μm was obtained.

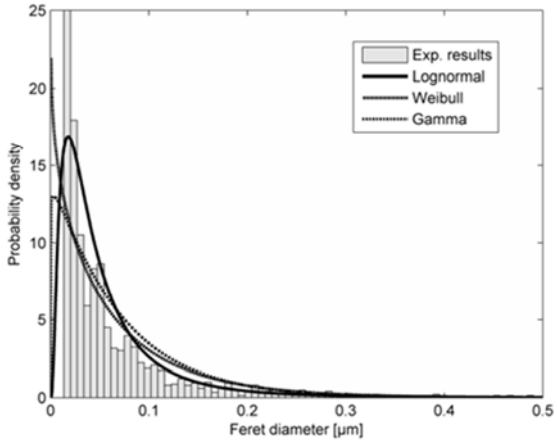

Figure 17. *PSD of activated carbon GAC250.*

4. Conclusion

A new procedure for quantitative characterization of different types of porous materials was proposed. The technique is based on the software *ImageJ* for processing the results of the SEM analysis. Thereby basic geometric features of the used materials such as pore size, grain size may be determined. In this study, the size of the solid particles, the average pore size and pore size distribution functions were obtained. Specifically the influence of the different parameters on the processing of SEM using specialized software *ImageJ* is considered. The procedure to obtain correct results on the basis of this analysis was proposed. In order to describe the experimental results, different distribution functions (Gamma, Weibull and Lognormal) were tested. On the basis of the obtained distributions, an average grain size L and an average macropore size D for different porous materials were determined for AC35 - $L = 60$ μm of $D = 0.6$ μm; ACENO - $L = 20$ μm of $D = 0.1$ μm; AX21 - $L = 30$ μm of $D = 0.1$ μm; IRH3 $D = 0.1$; GAC250 - $D = 0.05$ μm. In this study the lognormal distribution gave the best fit to the experimental data, followed by the Gamma distribution. Using the Weibull distribution, results with unsatisfactory accuracy were obtained.

In perspective of this work, establishment of a relation between the obtained pore distribution function and a specific surface area and a pore volume will permit to determine the values of these macroscopic solid properties. Thereby, SEM analyses enable to characterize porous solid structure (PSD, surface area and pore volume) without additional analysis methods such as adsorption-based techniques.

References

[1] K. Y. Foo, B. H. Hameed, Chem. Eng. J. 156 (2010) 2–10.

[2] M. Heuchel, D. Gerber, K. Kratz, A. Lendlein, Polym. Adv. Technol. (2016) doi: 10.1002/pat.3973.

[3] R. Guillet-Nicolas, R. Ahmad, K. A. Cychosz, F. Kleitz, M. Thommes, New Journal of Chemistry 40 (2016) 4351-4360.

[4] I. Suarez-Ruiz, International Journal of Coal Geology 159 (2016) 1-17.

[5] M. Lawrence, J. Yunhong, Bio-aggregates Based Building Materials. Springer Netherlands (2017) 39-71.

[6] S. Lowell, J. E. Shields, Powder Surface Area and Porosity, second ed. John, Wiley, New York, 1984.

[7] S. Brunauer, P. H. Emmet, F. Teller, J. Am. Chem. Soc. 60 (1938) 309-319.

[8] E. P. Barrett, L. G. Jayner, P. P. Hallenda, J. Am. Chem. Soc. 73 (1951) 373-380.

[9] G. Horvath, K. Kazakoe, J. Chem. Eng. Japan 16 (5) (1983) 470-475.

[10] A. F. AlMarzooqi, M. R. Bilad, B. M. Hassan, A. Arafat, Journal of materials science 51(4) (2016) 2017-2032.

[11] N. Marturi, B. Tamadazte, Sounkalo Dembele, IEEE Transactions on Instrumentation and Measurement 65(8) (2016) 1847-1855.

[12] T. Woehl, K. Robert, Ultramicroscopy 171 (2016), 166-176.

[13] J. Pascau, J. M. M. Pérez, Image Processing with ImageJ, September 2013, ISBN 13: 9781783283958.

[14] C. A. Schneider, W. S. Rasband, K. W. Eliceiri, Nat Methods 9 (7) (2012) 671-675.

[15] T. J. Collins, BioTechniques 43 (1 Suppl) (2007) 25-30 doi:10.2144/000112517.

[16] V. Girish, A. Vijayalakshmi, Indian J Cancer 41 (1) (2004) 47.

[17] C. T. Rueden, K. W. Eliceiri, BioTechniques 43 (1Suppl) (2007) 31 33–36.

[18] M. D. Abramoff, P. J. Magalhaes, S. J. Ram, Biophotonics International Laurin Publishing, Co. Inc., 2004.

[19] G. H. Kim, et al. Auris Nasus Larynx 44.2 (2017), 174-181.

[20] K. Eliceiri, C. T. Rueden, Photochem Photobiol 81 (5) (2005)22-1116.

[21] D. Barboriak, A. Padua, G. York, J. Macfall, J. Digit Imaging 18 (2) (2005) 9–91.

[22] T. C. Rueden, C. H. Mark, W. E. Kevin, Microscopy and Microanalysis 22. S3 (2016), 2066-2067.

[23] E. Gering, C. Atkinson, J. Parasitol 90 (4) (2004) 81-879.

[24] T. J. Collins, McMaster Biophotonics Facility, McMaster University, Hamilton, ON, Canada Bio Techniques 43(S1) (2007) 25–30.

[25] T. Ferreira, W. Rasband, "ImageJUserGuid", (2012) http://imagej.nih.gov/ij/docs/guide

[26] J. K. Vizietal, BMCBio informatics, 12(232) (2011).

[27] B. Schmid et al, BMCBio informatics 11(274) (2010).